Meccanica
DOI 10.1007/s11012-014-0011-1

Modelling inheritance of plastic deformation during migration of phase boundaries using a phase field method

Kais Ammar · Benoît Appolaire · Samuel Forest · Maeva Cottura · Yann Le Bouar · Alphonse Finel

Received: 26 May 2014 / Accepted: 26 June 2014

Abstract Recent advances in phase field modelling include the description of elastoviscoplastic material behaviour of the phases combined with diffusion and phase transformation. The corresponding models can be classified into two main groups of theories, referred to as interpolation and homogenisation models in the present work. It is shown that both approaches strongly differ concerning the question of inheritance of plastic deformation after the passing of a phase transformation front. Inheritance of plastic deformation is to be distinguished from the inheritance of the microstructure hardening and the corresponding dislocation structures. That is why the analysis is performed in the absence of hardening in the constitutive model. Finite element simulations of the growth of elastic misfitting precipitates embedded in a rate-independent elastoplastic matrix material reveal that the interpolation model allows for total inheritance of plastic deformation in contrast to the homogenisation model. The residual stress field and the growth kinetics are shown to be impacted by this essential property of the models. The results suggest that new models should be designed that allow for partial and controlled inheritance.

Keywords Phase field · Plasticity · Homogenization · Inheritance · Finite element

K. Ammar · S. Forest (✉)
Mines ParisTech, Centre des Matériaux / CNRS UMR 7633, BP 87, 91003 Evry Cedex, France
e-mail: samuel.forest@ensmp.fr

B. Appolaire · M. Cottura · Y. L. Bouar · A. Finel
Laboratoire d'Etude des Microstructures, CNRS/ONERA, UMR 104, BP 87, 92322 Châtillon Cedex, France

1 Introduction

The phase field approach currently emerges as a powerful method to simulate the evolution of microstructures under various thermodynamical and mechanical driving forces [35, 38]. Phase transformations are then treated within a field theory that provides both morphological changes of phases and the corresponding kinetics. The rôle of mechanics in this process has been seen to be essential in bringing additional potentially strong couplings with chemical processes [24]. This rôle has long been limited to elasticity effects, for instance in strain induced morphological transformations [41], although the importance of viscoplasticity was known from an experimental perspective [16, 30] or based on coupled diffusion and mechanics [7]. Recent advances of the phase field approach deal with the introduction of plastic and viscoplastic phenomena in addition to chemical and elastic processes [4, 5, 17, 18, 21, 34, 46]. Standard elastoviscoplastic nonlinear models of material behaviour are then incorporated in the form of additional time differential equations for internal

Published online: 29 August 2014

variables associated with dissipative processes [8, 29]. The coupling between elastoviscoplasticity and the phase field approach has been introduced according to two main model classes. In the first one, called the "interpolation model" in the present work, all material points are endowed with the same set of mechanical constitutive equations (including elasticity, von Mises plasticity or crystal plasticity, etc.) but the material parameters (including the elasticity moduli, the yield stress, the hardening modulus, etc.) differ in the phases and are interpolated within the diffuse interfaces [18, 21]. In the second model class, the phase field method is combined with the homogenisation approach well-known in the mechanics of heterogeneous materials [4, 5, 36, 37]. Arbitrary constitutive equations can then be used for each phase and homogenisation rules are applied to the free energy densities and dissipation potentials. The choice of the mixture rule has a significant influence on the behaviour of the diffuse interfaces, as recently discussed in [4, 12].

The question then arises of the evolution of plasticity-related variables at a material point after the passing of a phase transformation front. The question of inheritance of plastic deformation and hardening existing prior to phase transformation has already been addressed, although insufficiently, from the experimental perspective, for instance in the context of thermomechanical treatments [20] or the behaviour of TRIP steels [27]. But the question is largely open from the modelling point of view in the context of phase field approaches, despite preliminary attempts e.g. [1, 2, 28].

The question of inheritance of internal variables associated with plastic deformation when an interface sweeps a plastified zone of bulk phase, during migration of phase boundaries has not been discussed in most existing phase field models involving nonlinear material behaviour. The inheritance is likely to depend on the nature of the interface, but the question: "Does coherent and incoherent interface motion favor recovery of the hardening of the mother phase?" has no obvious answer, and will deserve a particular attention in the model development in order to reach realistic comparison with experimental results. Indeed, it is essential to know if the newly formed phase inherits all or part of the plastic strain or strain hardening of the parent phase, in order to predict the existence of residual stresses by structural calculations for instance.

It is first necessary to distinguish the question of inheritance of plastic deformation from that of strain hardening. Plastic deformation is associated with the motion of dislocations that do not necessarily stay in the material volume element and lead to a change of the local reference configuration for the calculation of elastic stresses. In contrast hardening is accompanied by the storage of dislocations that can be destroyed by the passing of a phase boundary or that can leave debris contributing to the hardening of the new phase. Alternatively, dislocations may be repelled by the moving interface. The mentioned previous references deal with the question of inheritance of strain hardening, i.e. of dislocation structures. In contrast, the question of inheritance of plastic deformation itself has not been addressed yet in the context of the recent advanced phase field models. The present work is limited to the consideration of this question, leaving the consideration of inheritance of strain hardening to future work. That is why the analysis is performed in the absence of hardening in the constitutive model.

The objective of the present work is to investigate the properties of existing phase field models with respect to the question of inheritance of plastic deformation during phase transformation. It will turn out that both classes of phase field models, namely the interpolation and homogenisation models, display strongly different plastic strain inheritance behaviours. The development of plastic deformation in the mother phase can be due to prior mechanical loading of the material or to local stresses induced by the misfit strain accompanying the motion of the phase transformation front. Inheritance can be total, partial or absent if the plastic strain tensor at the material point after the passing of the transformation front, is equal to that of the mother phase at that particular point, a portion of it or simply vanishing, respectively. In the case of total or partial inheritance the plastic residual shape of the structure is left totally or partially unchanged after the passing of a moving phase boundary. In contrast, the initial shape is completely recovered in the case of shape memory alloys for instance corresponding to no inheritance at all. The situation is more complicated in the case of plastic flow occurring during phase transformation due to external loading or local plastic deformation induced by high stresses

associated with transformation eigenstrains. The objective is then to study the impact of the choice of interpolation schemes on the inheritance of plastic deformation during phase transformation, depending on the particular class of phase field models. The analysis is limited to the small deformation framework for the sake of simplicity.

The formulation of both classes of phase field models is presented in Sect. 2, including the chemical and mechanical constitutive equations and the specific interpolation schemes characterising the diffuse interface response. Two simple situations are then considered in Sect. 3 to illustrate the inheritance behaviour of each class of models. They deal with the growth of elastic precipitates embedded in an elastoplastic matrix described by associated von Mises plasticity in the absence of hardening. For the same intrinsic nonlinear behaviour of individual phases, the concentration, plastic strain and stress fields will be shown to differ after precipitate growth depending on the phase field formulation.

In the following, intrinsic notations are used. Scalar, first, second and fourth ranks tensors are denoted by $a, \underline{\boldsymbol{a}}, \underline{\underline{\boldsymbol{a}}}$ and $\underline{\underline{\underline{\underline{a}}}}$, respectively. Simple and double contractions read $\cdot$ and :, respectively.

2 Model description

2.1 Balance equations

The governing equations of the coupled diffusion-phase transformation-mechanical problem are the mass balance for the conserved concentration field $c(\underline{\boldsymbol{x}}, t)$, the Ginzburg-Landau equation for the non-conserved order parameter $\phi(\underline{\boldsymbol{x}}, t)$, and the static equilibrium for the stress tensor $\underline{\underline{\boldsymbol{\sigma}}}(x, t)$ in the absence of volume forces:

$$\begin{aligned} &\dot{c} + \nabla.\left[-L(\phi)\left(\nabla\frac{\partial f}{\partial c}\right)\right] = 0 \\ &M\dot{\phi} - A\Delta\phi + \frac{\partial f}{\partial \phi} = 0 \\ &\nabla.\underline{\underline{\boldsymbol{\sigma}}} = 0 \end{aligned} \tag{1}$$

where M is the mobility parameter, f is Helmholtz free energy density and $L(\phi)$ is the Onsager coefficient in the case of isotropic materials.

2.2 Helmholtz free energy density

2.2.1 Partition of free energy

The total free energy F of the body is defined as the integral over the volume V of a free energy density f, which is split into a chemical free energy density contribution f_{ch}, a coherent mechanical energy density f_u, and a quadratic gradient contribution. Assuming that the free energy density depends on the order parameter ϕ, its gradient $\nabla\phi$, the concentration c, the elastic strain tensor $\underline{\underline{\boldsymbol{\varepsilon}}}^e$ and the set of internal variables V_k associated to material hardening, we have

$$\begin{aligned} F(\phi, \nabla\phi, c, \underline{\underline{\boldsymbol{\varepsilon}}}^e, V_k) &= \int_V f(\phi, \nabla\phi, c, \underline{\underline{\boldsymbol{\varepsilon}}}^e, V_k)\, dv \\ &= \int_V \left[f_{\text{ch}}(\phi, c) + f_u(\phi, c, \underline{\underline{\boldsymbol{\varepsilon}}}^e, V_k) + \frac{A}{2}|\nabla\phi|^2\right] dv \end{aligned} \tag{2}$$

where the usual quadratic isotropic Ginzburg term was chosen with respect to the gradient of the order parameter ϕ.

The total strain tensor $\underline{\underline{\boldsymbol{\varepsilon}}}$ is the symmetric part of the gradient of the displacement field. It is partitioned into the elastic strain $\underline{\underline{\boldsymbol{\varepsilon}}}^e$, the eigenstrain $\underline{\underline{\boldsymbol{\varepsilon}}}^\star$ due to phase transformation and the plastic strain $\underline{\underline{\boldsymbol{\varepsilon}}}^p$:

$$\underline{\underline{\boldsymbol{\varepsilon}}} = \underline{\underline{\boldsymbol{\varepsilon}}}^e + \underline{\underline{\boldsymbol{\varepsilon}}}^\star + \underline{\underline{\boldsymbol{\varepsilon}}}^p \tag{3}$$

2.2.2 Chemical contribution

Considering a two-phase binary alloy, the chemical free energy density f_{ch} of the binary alloy is a function of the order parameter ϕ and of the concentration field c. In order to guarantee the coexistence of both phases α and β discriminated by ϕ, f_{ch} must be non-convex with respect to ϕ. Following [25], f_{ch} is built with the free energy densities of the two individual phases f_α and f_β as follows:

$$f_{\text{ch}}(\phi, c) = h(\phi) f_\alpha(c) + \overline{h}(\phi) f_\beta(c) + W\Psi(\phi) \tag{4}$$

The subscripts α and β indicate the two coexisting phases. Here, the function $h(\phi) = 1 - \overline{h}(\phi)$ is taken as $h(\phi) = \phi^2(3 - 2\phi)$, and $\Psi(\phi) = \phi^2(1 - \phi)^2$ is the double well potential accounting for the free energy penalty of the interface. The height W of the potential

barrier is related to the interfacial energy γ and the interfacial thickness δ as $W = 6\Lambda\gamma/\delta$. Assuming that the interface region ranges from $\phi = \theta$ to $\phi = 1 - \theta$, then $\Lambda = \log((1-\theta)/\theta)$. In the present work $\theta = 0.05$ following [3, 25].

The densities f_α and f_β are chosen to be quadratic functions of the concentration only:

$$f_\alpha(c) = \frac{1}{2}k_\alpha(c - a_\alpha)^2 \quad \text{and} \quad f_\beta(c) = \frac{1}{2}k_\beta(c - a_\beta)^2 \tag{5}$$

The parameters k_α, k_β are the free energy curvatures with respect to concentration. They are assumed to be identical in the present study: $k_\alpha = k_\beta = k$. a_α and a_β are the equilibrium concentrations for α and β phases respectively [3].

2.2.3 *Mechanical contribution*

The second contribution to the free energy density in Eq. (2) is due to mechanical effects. Assuming that elastic behaviour and hardening are uncoupled, the mechanical part of the free energy density f_u is decomposed into a coherent elastic energy density f_e and a plastic part f_p as:

$$f_u(\phi, c, \underset{\sim}{\varepsilon}^e, V_k) = f_e(\phi, c, \underset{\sim}{\varepsilon}^e) + f_p(\phi, c, V_k) \tag{6}$$

The specific form of $f_u(\phi, c, \underset{\sim}{\varepsilon}^e, V_k)$ will be detailed in the next sections.

There are essentially two ways of introducing linear or nonlinear mechanical constitutive equations into the standard phase field approach, that are presented in the following.

2.3 Interpolation model

The material behaviour is described by a unified set of constitutive equations including material parameters that explicitly depend on the concentration or on the phase field variable. Each material parameter is usually interpolated between limit values known for each phase. This is the formulation adopted in the finite element simulations of Cahn-Hilliard like equations coupled with viscoplasticity by [6, 39, 40, 43] for tin-lead solders, also derived in [14, 15]. The same methodology is used in [17, 18] to simulate the rôle of viscoplasticity on rafting of γ' precipitates in single crystal nickel base superalloys under load. For instance, when an elastic phase coexists with an elastic-plastic one, the plastic yield threshold is interpolated between the actual value in the plastic phase and a very high unreachable value in the elastic phase, e.g. [10].

The diffuse interface behaviour resulting from this procedure can be compared to the ones commonly used in phase field models, as popularized by Khachaturyan and co-workers, e.g. [42]. According to the latter, mixture rules are adopted respectively for eigenstrain and the tensor of elasticity moduli:

$$\underset{\sim}{\varepsilon}^\star = \phi\,\underset{\sim}{\varepsilon}^\star_\alpha + (1-\phi)\,\underset{\sim}{\varepsilon}^\star_\beta, \quad \underset{\approx}{\boldsymbol{C}} = \phi\,\underset{\approx}{\boldsymbol{C}}_\alpha + (1-\phi)\,\underset{\approx}{\boldsymbol{C}}_\beta \tag{7}$$

where $\underset{\sim}{\varepsilon}^\star_{\alpha,\beta}$ and $\underset{\approx}{\boldsymbol{C}}_{\alpha,\beta}$ respectively are the eigenstrain and elasticity tensors of the individual phases. Hooke's law then relates the strain to the stress tensors by the following relations:

$$\begin{aligned}\underset{\sim}{\boldsymbol{\sigma}} &= \underset{\approx}{\boldsymbol{C}} : (\underset{\sim}{\varepsilon} - \underset{\sim}{\varepsilon}^\star) \\ &= (\phi\,\underset{\approx}{\boldsymbol{C}}_\alpha + (1-\phi)\,\underset{\approx}{\boldsymbol{C}}_\beta) : (\underset{\sim}{\varepsilon} - \phi\,\underset{\sim}{\varepsilon}^\star_\alpha - (1-\phi)\,\underset{\sim}{\varepsilon}^\star_\beta)\end{aligned} \tag{8}$$

In that way, the elastic energy of the effective homogeneous material at a material point cannot be interpreted as the average of energy densities of both phases [4, 5]. The elastic energy is then postulated as:

$$\begin{aligned}f_e(c, \underset{\sim}{\varepsilon}^e) &= \frac{1}{2}\,\underset{\sim}{\varepsilon}^e(c) : \underset{\approx}{\boldsymbol{C}}(c) : \underset{\sim}{\varepsilon}^e(c) \\ &= \frac{1}{2}\,(\underset{\sim}{\varepsilon} - \underset{\sim}{\varepsilon}^p - \underset{\sim}{\varepsilon}^\star(c)) : \underset{\approx}{\boldsymbol{C}}(c) : (\underset{\sim}{\varepsilon} - \underset{\sim}{\varepsilon}^p - \underset{\sim}{\varepsilon}^\star(c))\end{aligned} \tag{9}$$

where the explicit concentration dependence of material parameters has been introduced. The second term f_p in (6) accounts for mechanical energy contributions due to hardening effects. Plastic or viscoplastic deformation is generally associated with dislocation storage and therefore energy storage to be included in the free energy density. We consider here that the system consists of a two-phase elastoplastic binary alloy with one non-linear isotropic hardening and one non-linear kinematic hardening in each phase, following standard formulations of elastoviscoplastic constitutive equations [8, 29]. The specific plastic free energy is chosen as a quadratic function of all state variables:

$$f_p(\phi, c, \underset{\sim}{\boldsymbol{\alpha}}, r) = \frac{1}{3} H(\phi, c) \underset{\sim}{\boldsymbol{\alpha}} : \underset{\sim}{\boldsymbol{\alpha}} + \frac{1}{2} b(\phi, c) Q(\phi, c) r^2 \tag{10}$$

where $\underset{\sim}{\boldsymbol{\alpha}}$ and r respectively are a tensorial kinematic and a scalar isotropic hardening variable, and H, Q and b are material parameters. In particular, H represents a plastic kinematic hardening modulus whereas the meaning of Q and b will become apparent at the end of this section. Each parameter is interpolated between limit values known for each phase as follows:

$$\begin{cases} c = \phi\, c_\alpha + (1-\phi)\, c_\beta \\ b = \phi\, b_\alpha + (1-\phi)\, b_\beta \\ Q = \phi\, Q_\alpha + (1-\phi)\, Q_\beta \end{cases} \tag{11}$$

A yield criterion $g(\phi, c)$ is introduced:

$$g(\underset{\sim}{\boldsymbol{\sigma}}, \underset{\sim}{\boldsymbol{X}}, R, \phi) = \sigma^{\mathrm{eq}}(\underset{\sim}{\boldsymbol{\sigma}}, \underset{\sim}{\boldsymbol{X}}) - \sigma^0 - R(\phi) \qquad \text{with}$$
$$R(\phi) = \phi\, R_\alpha + (1-\phi)\, R_\beta \tag{12}$$

where σ^0 is the initial yield stress and R subsequent isotropic hardening according to

$$R = \frac{\partial f_p}{\partial r} = bQ\, r \tag{13}$$

As a result, $\sigma^0 + R$ is the radius of the elasticity domain. The function σ^{eq} is chosen as the von Mises equivalent stress measure:

$$\sigma^{\mathrm{eq}} = \sqrt{\frac{3}{2}(\underset{\sim}{\boldsymbol{s}} - \underset{\sim}{\boldsymbol{X}}) : (\underset{\sim}{\boldsymbol{s}} - \underset{\sim}{\boldsymbol{X}})}, \quad \text{with}$$
$$\underset{\sim}{\boldsymbol{s}} = \underset{\sim}{\boldsymbol{\sigma}} - \frac{1}{3}(\mathrm{trace}\, \underset{\sim}{\boldsymbol{\sigma}})\underset{\sim}{\boldsymbol{I}} \tag{14}$$

The tensors $\underset{\sim}{\boldsymbol{s}}$ and $\underset{\sim}{\boldsymbol{X}}$ respectively are the deviatoric stress tensor and the back-stress tensor accounting for kinematic hardening:

$$\underset{\sim}{\boldsymbol{X}} = \frac{\partial f_p}{\partial \underset{\sim}{\boldsymbol{\alpha}}} = \frac{2}{3} H \underset{\sim}{\boldsymbol{\alpha}} \tag{15}$$

According to the normality rule, the plastic flow rule takes the form

$$\dot{\underset{\sim}{\boldsymbol{\varepsilon}}}^p = \dot{\lambda} \frac{\partial g}{\partial \underset{\sim}{\boldsymbol{\sigma}}} = \dot{\lambda} \underset{\sim}{\boldsymbol{n}} \tag{16}$$

where the direction of plastic flow is $\underset{\sim}{\boldsymbol{n}} = 3/2\, \underset{\sim}{\boldsymbol{s}} / \sigma^{\mathrm{eq}}$ in the case of the von Mises criterion and $\dot{\lambda}$ is the plastic multiplier. The evolution laws for isotropic and kinematic variables can be taken, for instance, from Chaboche model [8]:

$$\dot{r} = \dot{\lambda}\left(1 - \frac{R}{Q}\right) = \dot{\lambda}(1 - br), \quad \text{and}$$
$$\dot{\underset{\sim}{\boldsymbol{\alpha}}} = \dot{\lambda}\left(\underset{\sim}{\boldsymbol{n}} - \frac{3\Gamma}{2H} \underset{\sim}{\boldsymbol{X}}\right) \tag{17}$$

Nonlinear kinematic hardening is characterized by the additional material parameter Γ.

In the case of rate-independent plasticity considered here for simplicity, the plastic multiplier $\dot{\lambda}$ is determined from the consistency condition $dg/dt = 0$ and $g = 0$ under plastic loading condition[1]

2.4 Multiphase approach: homogenisation method

An alternative approach for formulating mechanical constitutive equations within a phase field framework is to resort to the multiphase approach as initially proposed in [35, 36, 38]. Within this framework, it is possible to apply some results of the homogenisation theory developed in the mechanics of heterogeneous materials [8, 33, 45] as demonstrated in [4, 5, 12].

One distinct set of constitutive equations is attributed to each individual phase α, β. Each phase at a material point then possesses its own stress/strain tensors $\underset{\sim}{\boldsymbol{\sigma}}_{\alpha,\beta}$, $\underset{\sim}{\boldsymbol{\varepsilon}}_{\alpha,\beta}$. The overall strain and stress quantities $\underset{\sim}{\boldsymbol{\sigma}}$, $\underset{\sim}{\boldsymbol{\varepsilon}}$ at this material point are defined as the averages of the corresponding tensors attributed to each phase. This is particularly important for points inside the smooth interface zone. At this stage, several homogenisation rules are available to perform the averaging. This homogenisation rule can also be interpreted as specific interpolation relations since there is generally no clear physical picture of the distribution of phases at the atomic scale underlying each material point of the diffuse interface. The advantage of the approach is that it makes it possible to mix strongly different types of constitutive equations for each phase, like hyperelastic nonlinear behaviour for one phase and conventional elasto-plastic model

[1] The first condition, $g = 0$, means that the state of stress is on the actual yield surface, the second $\dot{g} = 0$ is the continuing plastic loading condition. Elastic unloading occurs when $g < 0$ or $\dot{g} < 0$, the internal variables then keeping a constant value.

with internal variables for the other one. No correspondence of material parameters is needed between the respective constitutive laws of the phases. This is the approach proposed in [36] for incorporating elasticity in a multi-phase field model. For that purpose, the authors resorted to a well-known homogeneous stress hypothesis (Reuss model) taken from homogenisation theory in the mechanics of heterogeneous materials [31, 32]. This approach has been applied to compute the effect of chemically induced strain on pearlite growth kinetics in [37].

It must be emphasised that this procedure is very similar to what has already been proposed for handling diffusion in phase field models [26]. Two concentration fields c_α and c_β are indeed introduced, and the real concentration field is obtained by a mixture rule together with an internal constraint on the diffusion potentials, called quasi-equilibrium constraint in [13]. Introducing two concentration fields gives an additional degree of freedom for controlling the energy of the interface with respect to its thickness. Furthermore, the chemical and mechanical coupling inside the diffuse interface sometimes leads to spurious effects like too high stresses or stress fluctuation, due to the often unrealistic interface thickness that one is forced to use in practical applications. Adding additional degrees of freedom like fictitious concentration or other state variables for describing the stress/strain behaviour within a diffuse interface can be useful to to get rid of such unwanted behaviour.

The homogenisation procedure in the mechanics of heterogeneous materials consists in replacing an heterogeneous medium by an equivalent homogeneous one, which is defined by an effective constitutive law relating the macroscopic variables, namely macroscopic stress $\underset{\sim}{\boldsymbol{\sigma}}$ and strain $\underset{\sim}{\boldsymbol{\varepsilon}}$ tensors, which are obtained by averaging the corresponding non-uniform local stress and strain in each phase. In the case of two-phase materials:

$$\underset{\sim}{\boldsymbol{\varepsilon}} = \frac{1}{\mathcal{V}} \sum_{k=\alpha,\beta} \int_{\mathcal{V}_k} \underset{\sim}{\boldsymbol{\varepsilon}}_k \, dv \quad \text{and} \quad \underset{\sim}{\boldsymbol{\sigma}} = \frac{1}{\mathcal{V}} \sum_{k=\alpha,\beta} \int_{\mathcal{V}_k} \underset{\sim}{\boldsymbol{\sigma}}_k \, dv \tag{18}$$

where $\mathcal{V} = \mathcal{V}_\alpha \cup \mathcal{V}_\beta$ is the underlying material representative volume element (RVE). In many cases, the actual geometry of the RVE is left unspecified but, for instance, the homogenisation scheme used in the phase-field/microelasticity approach in [12], corresponds to a laminate microstructure of the interface. Following a simple representation depicted in Fig. 1, each material point, i.e. $\mathcal{V}$, within a diffuse interface can be seen as a local mixture of the two abutting phases α and β with proportions fixing $\mathcal{V}_\alpha$ and $\mathcal{V}_\beta$ given by complementary functions of ϕ.

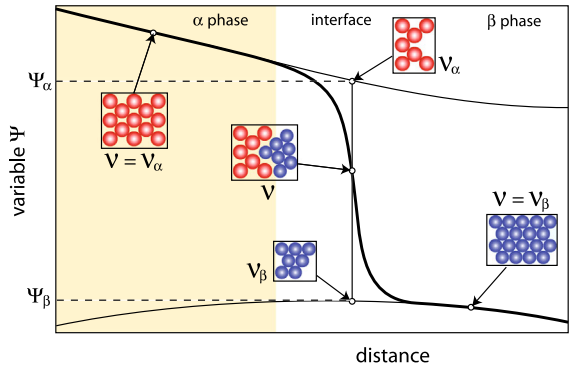

Fig. 1 Schematic illustration of the underlying material representative volume element $\mathcal{V}$ at each material point of a diffuse interface: The real effective variable Ψ appears with a thick line, whereas the variables attached to each phase Ψ_α and Ψ_β are with thinner lines

In the case of a two-phase material, the strain and stress at each material point are defined by the following mixture laws which would proceed from space averaging in a conventional homogenisation problem, but which can be seen as interpolations in the present case:

$$\underset{\sim}{\boldsymbol{\varepsilon}} = h(\phi)\, \underset{\sim}{\boldsymbol{\varepsilon}}_\alpha + \overline{h}(\phi)\, \underset{\sim}{\boldsymbol{\varepsilon}}_\beta \quad \text{and} \quad \underset{\sim}{\boldsymbol{\sigma}} = h(\phi)\, \underset{\sim}{\boldsymbol{\sigma}}_\alpha + \overline{h}(\phi)\, \underset{\sim}{\boldsymbol{\sigma}}_\beta \tag{19}$$

where $\underset{\sim}{\boldsymbol{\varepsilon}}_\alpha, \underset{\sim}{\boldsymbol{\varepsilon}}_\beta$ are the local strains and $\underset{\sim}{\boldsymbol{\sigma}}_\alpha, \underset{\sim}{\boldsymbol{\sigma}}_\beta$ are the local stresses attributed, at a material point, to the α and β phases respectively, and $h(\phi)$ is a polynomial function varying in a monotonic way from 0 to 1 between both phases, as usual in phase field approaches. Note that in homogenisation theory, one has $h(\phi) = \phi$ which turns out to be insufficient for the modelling of evolving microstructures.

According to the homogenisation theory, the effective elastic and plastic free energy densities are given by the rule of mixtures as follows:

$$f_e(\phi, c, \underset{\sim}{\boldsymbol{\varepsilon}}^e_\alpha, \underset{\sim}{\boldsymbol{\varepsilon}}^e_\beta) = h(\phi) f_{e\alpha}(c, \underset{\sim}{\boldsymbol{\varepsilon}}^e_\alpha) + \overline{h}(\phi) f_{e\beta}(c, \underset{\sim}{\boldsymbol{\varepsilon}}^e_\beta) \tag{20}$$

$$f_p(\phi, c, V_{k\alpha}, V_{k\beta}) = h(\phi) f_{p\alpha}(c, V_{k\alpha}) + \overline{h}(\phi) f_{p\beta}(c, V_{k\beta}) \tag{21}$$

All state and internal variables are therefore duplicated and corresponding variables $\underset{\sim}{\varepsilon}^{e}{}_{\alpha,\beta}$ and $V_{k\alpha,\beta} V_{k\alpha,\beta}$ are introduced.

In the proposed model, the reversible mechanical behaviour of each individual phase is governed by a convex mechanical free energy potential, which can be decomposed, using Eq. (6), into the contributions of each phase.

2.4.1 Elastic energy density

The effective elastic energy is expressed in terms of the elastic energies of both phases weighted by the complementing functions $h(\phi)$ and $\overline{h}(\phi)$. The corresponding free energy densities $f_{e\alpha}, f_{e\beta}$ are introduced as quadratic potentials with respect to the elastic strain contributions of the different phases:

$$f_e = h(\phi) f_{e\alpha} + \overline{h}(\phi) f_{e\beta} \tag{22}$$

with

$$f_{e\alpha}(\underset{\sim}{\varepsilon}^{e}_{\alpha}) = \frac{1}{2} \underset{\sim}{\varepsilon}^{e}_{\alpha} : \underset{\approx}{C}_{\alpha} : \underset{\sim}{\varepsilon}^{e}_{\alpha} \qquad \text{and}$$
$$f_{e\beta}(\underset{\sim}{\varepsilon}^{e}_{\beta}) = \frac{1}{2} \underset{\sim}{\varepsilon}^{e}_{\beta} : \underset{\approx}{C}_{\beta} : \underset{\sim}{\varepsilon}^{e}_{\beta} \tag{23}$$

where the fourth-order tensors of elasticity moduli, $(\underset{\approx}{C}_{\alpha}, \underset{\approx}{C}_{\beta})$, of the individual phases are introduced.

The total strains, $(\underset{\sim}{\varepsilon}_{\alpha}, \underset{\sim}{\varepsilon}_{\beta})$, the eigenstrains, $(\underset{\sim}{\varepsilon}^{\star}_{\alpha}, \underset{\sim}{\varepsilon}^{\star}_{\beta})$ and the plastic strain tensors $(\underset{\sim}{\varepsilon}^{p}_{\alpha}, \underset{\sim}{\varepsilon}^{p}_{\beta})$ are introduced for both phases at each material point of the whole body. The partition hypothesis, already used for the effective total strain tensor in (3), requires, in a similar way, a decomposition of the total strain in each phase into elastic, eigenstrain and plastic parts:

$$\underset{\sim}{\varepsilon}_{\alpha} = \underset{\sim}{\varepsilon}^{e}_{\alpha} + \underset{\sim}{\varepsilon}^{\star}_{\alpha} + \underset{\sim}{\varepsilon}^{p}_{\alpha} \quad \text{and} \quad \underset{\sim}{\varepsilon}_{\beta} = \underset{\sim}{\varepsilon}^{e}_{\beta} + \underset{\sim}{\varepsilon}^{\star}_{\beta} + \underset{\sim}{\varepsilon}_{\beta} \tag{24}$$

The eigenstrains and tensors of elastic moduli at each point may then depend on the local concentration c, but not on the order parameter ϕ.

At this stage, the Voigt/Taylor assumption from homogenisation theory is introduced stating that

$$\underset{\sim}{\varepsilon}_{\alpha} = \underset{\sim}{\varepsilon}_{\beta} = \underset{\sim}{\varepsilon} \tag{25}$$

so that the local Hooke laws take the form

$$\underset{\sim}{\sigma}_{\alpha} = \underset{\approx}{C}_{\alpha} : (\underset{\sim}{\varepsilon} - \underset{\sim}{\varepsilon}^{\star}_{\alpha} - \underset{\sim}{\varepsilon}^{p}_{\alpha}), \quad \underset{\sim}{\sigma}_{\beta} = \underset{\approx}{C}_{\beta} : (\underset{\sim}{\varepsilon} - \underset{\sim}{\varepsilon}^{\star}_{\beta} - \underset{\sim}{\varepsilon}^{p}_{\beta}) \tag{26}$$

The resulting global Hooke law follows from the averaging rule (19):

$$\underset{\sim}{\sigma} = h(\phi) \underset{\approx}{C}_{\alpha} : (\underset{\sim}{\varepsilon} - \underset{\sim}{\varepsilon}^{\star}_{\alpha} - \underset{\sim}{\varepsilon}^{p}_{\alpha}) + \overline{h}(\phi) \underset{\approx}{C}_{\beta} : (\underset{\sim}{\varepsilon} - \underset{\sim}{\varepsilon}^{\star}_{\beta} - \underset{\sim}{\varepsilon}^{p}_{\beta}) \tag{27}$$

It can be rewritten in the following form:

$$\underset{\sim}{\sigma} = \underset{\approx}{C}_{\text{eff}} : (\underset{\sim}{\varepsilon} - \underset{\sim}{\varepsilon}^{p} - \underset{\sim}{\varepsilon}^{\star}) \tag{28}$$

where the effective elasticity moduli $\underset{\approx}{C}_{\text{eff}}$, effective eigenstrain $\underset{\sim}{\varepsilon}^{\star}$ and effective plastic strain $\underset{\sim}{\varepsilon}^{p}$ are defined as

$$\underset{\approx}{C}_{\text{eff}} = h(\phi)\, \underset{\approx}{C}_{\alpha} + \overline{h}(\phi)\, \underset{\approx}{C}_{\beta} \tag{29}$$

$$\underset{\sim}{\varepsilon}^{\star} = \underset{\approx}{C}^{-1}_{\text{eff}} : (h(\phi)\, \underset{\approx}{C}_{\alpha} : \underset{\sim}{\varepsilon}^{\star}_{\alpha} + \overline{h}(\phi)\, \underset{\approx}{C}_{\beta} : \underset{\sim}{\varepsilon}^{\star}_{\beta}) \tag{30}$$

$$\underset{\sim}{\varepsilon}^{p} = \underset{\approx}{C}^{-1}_{\text{eff}} : (h(\phi)\, \underset{\approx}{C}_{\alpha} : \underset{\sim}{\varepsilon}^{p}_{\alpha} + \overline{h}(\phi)\, \underset{\approx}{C}_{\beta} : \underset{\sim}{\varepsilon}^{p}_{\beta}) \tag{31}$$

which are the well-known Voigt effective properties. Note that (30) and (31) differ from usual phase field schemes as discussed in [4].

2.4.2 Plastic energy density

Considering the case of a two-phase elastoplastic alloy, it is considered that energy can be stored due to non-linear isotropic hardening and non-linear kinematic hardening in each phase. The hardening components are modelled by means of internal variables attributed to each phase. The set of internal variables V_k, of scalar or tensorial nature, represents the state of hardening of phase k: for instance, a scalar isotropic hardening variable r_k, and a tensorial kinematic hardening variable $\underset{\sim}{\alpha}_k$

$$V_k = \left\{ r_{\alpha}, r_{\beta}, \underset{\sim}{\alpha}_{\alpha}, \underset{\sim}{\alpha}_{\beta} \right\} \tag{32}$$

The associated thermodynamic driving forces are

$$R_\alpha = \frac{\partial f_{p\alpha}}{\partial r_\alpha}, \quad R_\beta = \frac{\partial f_{p\beta}}{\partial r_\beta}, \quad \underset{\sim}{\boldsymbol{X}}_\alpha = \frac{\partial f_{p\alpha}}{\partial \underset{\sim}{\boldsymbol{\alpha}}_\alpha}, \quad \underset{\sim}{\boldsymbol{X}}_\beta = \frac{\partial f_{p\beta}}{\partial \underset{\sim}{\boldsymbol{\alpha}}_\beta} \tag{33}$$

A simple quadratic potential is adopted for the plastic part of the free energy density:

$$\begin{aligned} f_\alpha^p &= \frac{1}{3} H_\alpha \underset{\sim}{\boldsymbol{\alpha}}_\alpha : \underset{\sim}{\boldsymbol{\alpha}}_\alpha + \frac{1}{2} b_\alpha Q_\alpha r_\alpha^2, \\ f_\beta^p &= \frac{1}{3} H_\beta \underset{\sim}{\boldsymbol{\alpha}}_\beta : \underset{\sim}{\boldsymbol{\alpha}}_\beta + \frac{1}{2} b_\beta Q_\beta r_\beta^2 \end{aligned} \tag{34}$$

thus assuming that each phase exhibits the same kind of isotropic elastoplastic behaviour, which is a simplification but not a real restriction in the approach. These potentials are similar to the function (10) chosen in the multiphase approach but different values of the constant material parameters $b_{\alpha,\beta}, Q_{\alpha,\beta}$ and $H_{\alpha,\beta}$ are attributed to each phase. These parameters may depend on the concentration c but they do not depend on ϕ. It follows from (34) and (33) that

$$R_\alpha = b_\alpha Q_\alpha r_\alpha, \quad R_\beta = b_\beta Q_\beta r_\beta \tag{35}$$

$$\underset{\sim}{\boldsymbol{X}}_\alpha = \frac{2}{3} H_\alpha \underset{\sim}{\boldsymbol{\alpha}}_\alpha, \quad \underset{\sim}{\boldsymbol{X}}_\beta = \frac{2}{3} H_\beta \underset{\sim}{\boldsymbol{\alpha}}_\beta \tag{36}$$

Still assuming that the elastoplastic behaviour of each phase is treated independently, distinct yield functions are introduced for both phases as

$$\begin{aligned} g_\alpha(\sigma_\alpha, \underset{\sim}{\boldsymbol{X}}_\alpha, R_\alpha) &= \sigma_\alpha^{\mathrm{eq}} - R_\alpha - \sigma_\alpha^0, \\ g_\beta(\sigma_\beta, \underset{\sim}{\boldsymbol{X}}_\beta, R_\beta) &= \sigma_\beta^{\mathrm{eq}} - R_\beta - \sigma_\beta^0 \end{aligned} \tag{37}$$

The parameters $\sigma_{\alpha,\beta}^0$ represent the initial yield stress of each phase. In the present work, a von Mises criterion is adopted for both phases:

$$\begin{aligned} \sigma_\alpha^{\mathrm{eq}} &= \sqrt{\frac{3}{2} (\underset{\sim}{\boldsymbol{s}}_\alpha - \underset{\sim}{\boldsymbol{X}}_\alpha) : (\underset{\sim}{\boldsymbol{s}}_\alpha - \underset{\sim}{\boldsymbol{X}}_\alpha)} \quad \text{where} \\ \underset{\sim}{\boldsymbol{s}}_\alpha &= \underset{\sim}{\boldsymbol{\sigma}}_\alpha - \frac{1}{3} (\mathrm{trace}\, \underset{\sim}{\boldsymbol{\sigma}}_\alpha) \underset{\sim}{\boldsymbol{1}} \end{aligned} \tag{38}$$

$$\begin{aligned} \sigma_\beta^{\mathrm{eq}} &= \sqrt{\frac{3}{2} (\underset{\sim}{\boldsymbol{s}}_\beta - \underset{\sim}{\boldsymbol{X}}_\beta) : (\underset{\sim}{\boldsymbol{s}}_\beta - \underset{\sim}{\boldsymbol{X}}_\beta)} \quad \text{where} \\ \underset{\sim}{\boldsymbol{s}}_\beta &= \underset{\sim}{\boldsymbol{\sigma}}_\beta - \frac{1}{3} (\mathrm{trace}\, \underset{\sim}{\boldsymbol{\sigma}}_\beta) \underset{\sim}{\boldsymbol{1}} \end{aligned} \tag{39}$$

where the deviatoric stress tensors $\underset{\sim}{\boldsymbol{s}}_{\alpha,\beta}$ are introduced.

The plastic flow rules and the evolution equations for the internal variables are the following:

$$\dot{\underset{\sim}{\boldsymbol{\varepsilon}}}_\alpha^p = \dot{\lambda}_\alpha \underset{\sim}{\boldsymbol{n}}_\alpha, \quad \text{with} \quad \underset{\sim}{\boldsymbol{n}}_\alpha = \frac{\partial g_\alpha}{\partial \underset{\sim}{\boldsymbol{\sigma}}_\alpha} \tag{40}$$

$$\dot{\underset{\sim}{\boldsymbol{\varepsilon}}}_\beta^p = \dot{\lambda}_\beta \underset{\sim}{\boldsymbol{n}}_\beta, \quad \text{with} \quad \underset{\sim}{\boldsymbol{n}}_\beta = \frac{\partial g_\beta}{\partial \underset{\sim}{\boldsymbol{\sigma}}_\beta} \tag{41}$$

$$\dot{r}_\alpha = \dot{\lambda}_\alpha \left(1 - \frac{R_\alpha}{Q_\alpha}\right), \quad \dot{r}_\beta = \dot{\lambda}_\beta \left(1 - \frac{R_\beta}{Q_\beta}\right) \tag{42}$$

$$\dot{\underset{\sim}{\boldsymbol{\alpha}}}_\alpha = \dot{\lambda}_\alpha \left(\underset{\sim}{\boldsymbol{n}}_\alpha - \frac{3\Gamma_\alpha}{2C_k} \underset{\sim}{\boldsymbol{X}}_\alpha\right), \quad \dot{\underset{\sim}{\boldsymbol{\alpha}}}_\alpha = \dot{\lambda}_\alpha \left(\underset{\sim}{\boldsymbol{n}}_\alpha - \frac{3\Gamma_\alpha}{2C_k} \underset{\sim}{\boldsymbol{X}}_\alpha\right) \tag{43}$$

As a result, two distinct plastic multipliers $\dot{\lambda}_{\alpha,\beta}$ are required in the theory. They are determined independently for each phase using the consistency condition in rate-independent elastoplasticity.

3 Results

The two presented phase field approaches, namely the interpolation and homogenisation models, have been applied to study the mechanical effect on the diffusion-controlled growth of α-precipitates embedded in a supersaturated β-matrix phase. The particles and matrix are separated by a coherent diffuse interface endowed with the constitutive properties described in the previous sections. The case of a single spherical precipitate is considered first, before studying the coalescence of a collection of initially circular precipitates. Internal stresses are generated by the transformation eigenstrains. To ease the interpretation of the results, the α phase displays a purely elastic behaviour whereas the β phase is assumed to be elastic-perfectly plastic with a yield stress σ_β^0. Homogeneous isothermal isotropic mechanical behaviour is considered for both phases.

3.1 Conditions of the finite element calculations

The previous models have been implemented into the finite element code Z-set [44]. The variational formulation corresponding to the field equations (1) and the implicit resolution schemes based on a monolithic framework are described in [3, 5].

All chemical and mechanical material data values are dimensionless and scaled with the chemical free energy curvature, which is chosen to be the same for

both phases ($k_\alpha = k_\beta = k$), a mesoscopic system length r_0, where r_0 is the initial radius of the precipitates, and the characteristic time $\tau = M/k$. Identical chemical diffusivities $D_{\alpha,\beta}$ are assumed in the two phases. They are taken such that $D\,\tau/r_0^2 = 1 \times 10^{-4}$. The interfacial energy is isotropic, $\gamma/(kr_0) = 5 \times 10^{-3}$. The corresponding interface thickness has been chosen to be about 0.5 % of the total size of the system $\delta/r_0 = 0.25$. The equilibrium concentrations at incoherent state for both phases are $a_\alpha = 0.7$ and $a_\beta = 0.3$. Both phases possess the same isotropic normalized elastic moduli, corresponding to a Young modulus $E/k = 7 \times 10^{10}$ and a Poisson ratio ν= 0.3. For the sake of simplicity, the eigenstrains in both phases are spherical tensors independent of concentration. Taking the β phase as the stress free reference state ($\underset{\sim}{\boldsymbol{\varepsilon}}_\beta^\star = \underset{\sim}{\boldsymbol{0}}$), the eigenstrain in the α phase is a spherical tensor ($\underset{\sim}{\boldsymbol{\varepsilon}}_\alpha^\star = \varepsilon_\alpha^\star \underset{\sim}{\mathbf{1}} = 6 \cdot 10^{-4} \underset{\sim}{\mathbf{1}}$).

The normalized yield stress for the β phase is $\sigma_\beta^0/k = 12$.

Circular nuclei of α phase are introduced in the β-matrix as initial conditions for the phase field ϕ. The initial condition for the concentration field is a uniform equilibrium value of c_α in the nuclei and the precipitate grows under a matrix supersaturation ($c_\beta^\infty - c_\beta^{\text{int}}$). Neglecting effects of interfacial curvature and in complete absence of stress field, the interfacial concentrations c_α^{int} and c_β^{int} correspond to the equilibrium concentrations for the specified phase obtained from the phase diagram. A typical composition profile is shown schematically in Fig. 2 for the single precipitate studied in the next subsection.

The concentration field within the matrix is given in [9], verifying the following interface/boundary conditions for the composition field:

$$\begin{aligned} c_\beta &= c_\beta^{\text{int}} \qquad \text{when} \qquad x = x_{int}^+ \\ c_\beta &= c_\infty \qquad \text{when} \qquad x \to \infty \end{aligned} \tag{44}$$

$c_\beta^\infty$is the far-field matrix concentration, which is assumed to be independent of time in the case of the isolated precipitate.

3.2 Growth of a spherical precipitate

In this section, the case of an isolated misfitting spherical precipitate in a supersaturated matrix is chosen in order to compare the proposed phase field mechanical models and examine the stored mechanical energy effect on the interfacial compositions and the diffusion-controlled growth. Interfacial conditions for mechanical equilibrium in two-phase crystals separated by a curved interface are deduced.

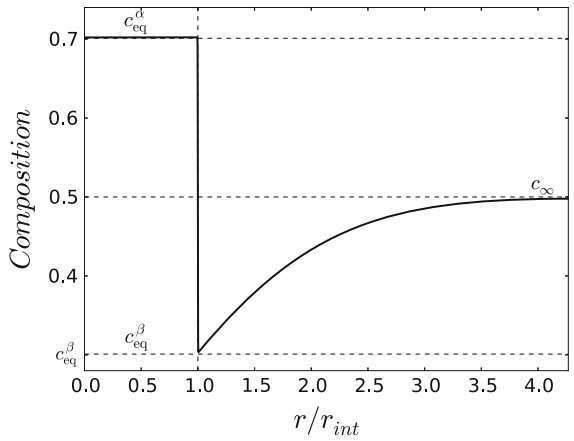

Fig. 2 Schematic illustration of the composition profile at a given time associated with the growth of an isolated coherent precipitate into a supersaturated matrix. The matrix/precipitate interface lies at $r/r_{\text{int}} = 1, r_{int}$ being the current position of the interface.

The geometry of the problem is that of two concentric spheres, the central one delimiting the α precipitate, the outer one corresponding to the outer surface of the β matrix. The computation is made by means of axisymmetric finite elements with a finite element mesh corresponding to one sector $0 \le \theta \le \theta_0 = 10°$. The initial spherical nucleus has a radius r_0 whereas the outer boundary of the matrix is at $r = R$. The finite element mesh is composed of linear 4-node axisymmetric quadrangular elements.

Profiles of ϕ and c as tanh functions along one direction have been set initially, which correspond to coexistence of an initial misfitting spherical precipitate of initial radius $r_0/R = 0.02$, and a β matrix of outer radius R and separated by a curved diffuse interface with a thickness roughly equal to δ. Let us call $\mathcal{S}$ the union of the surfaces $r = R$, $\theta = 0$ and $\theta = \theta_0$. The following boundary conditions have been applied to the system:

$$\begin{aligned} &\underline{\boldsymbol{\xi}}.\underline{\boldsymbol{n}} = 0, \quad \underline{\boldsymbol{J}}.\underline{\boldsymbol{n}} = 0 && \text{on the surface } \mathcal{S} \\ &\sigma_{rr}(r = R) = 0 && \text{free surface condition} \\ &u_\theta = 0 && \text{on the surface } \mathcal{S} \end{aligned} \tag{45}$$

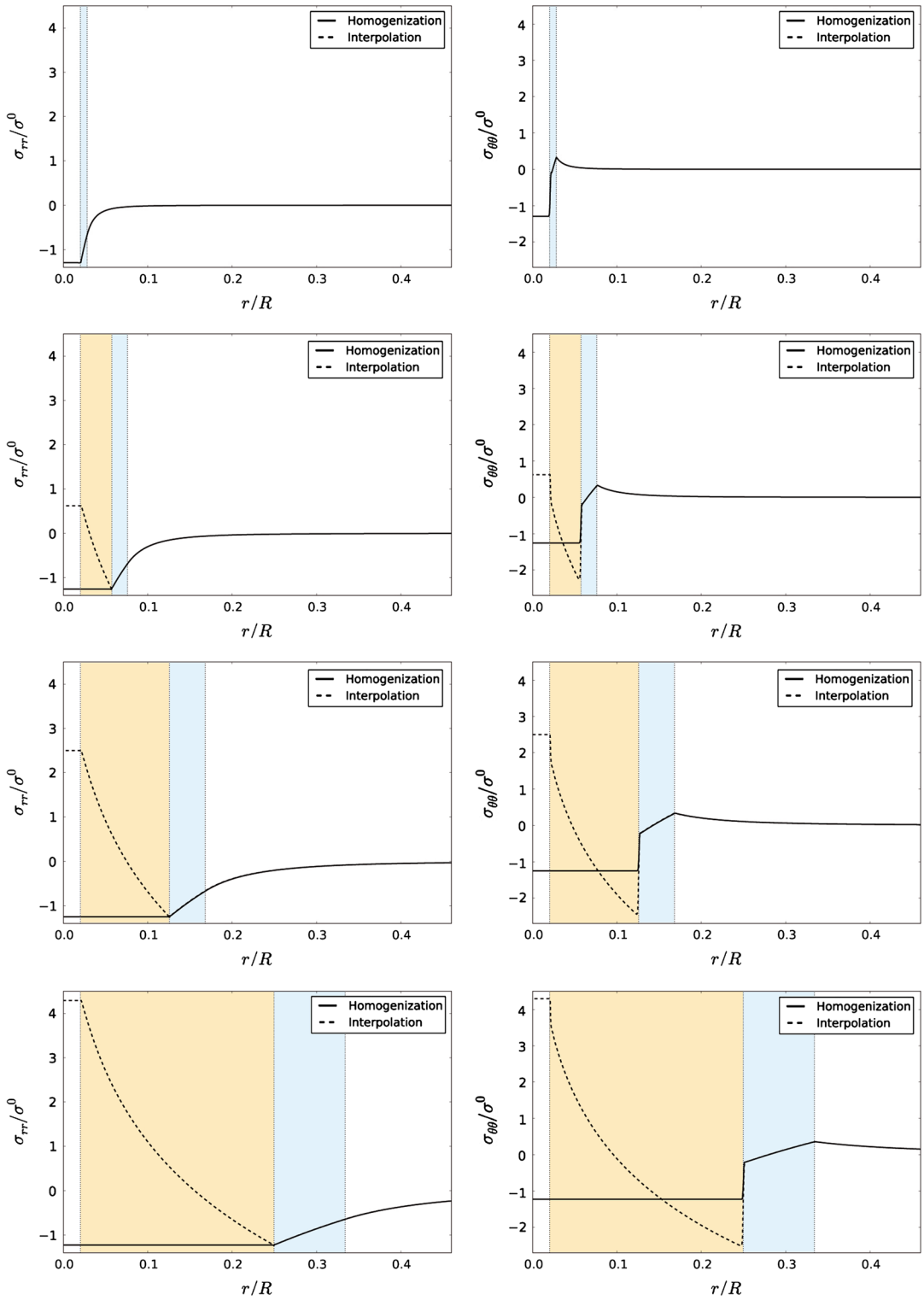
Homogenization
Interpolation
σ_{rr}/σ^0
$\sigma_{\theta\theta}/\sigma^0$
r/R

◀**Fig. 3** Normal σ_{rr} and tangential $\sigma_{\theta\theta}$ stress distributions in a radial direction from the center of the particle with both interpolation and homogenisation methods, at four stages of the growth process. Stresses are normalized with respect to the yield stress σ^0_β. The matrix precipitate interface lies at $r/r_{int} = 1$. The white, brown and blue colors respectively correspond to the initial nucleus, grown α phase domain, and active plastic zone in the matrix.

where $\underline{\boldsymbol{n}}$ is the normal vector to the considered surface. The generalized stress vector $\underline{\boldsymbol{\xi}} = A\nabla\phi$ is defined in [3, 22].

Figure 3 compares the stress distributions in a misfitting spherical precipitate, obtained in the case of ideal plastic deformation in the matrix according to the interpolation and homogenisation methods. The radial stress σ_{rr} and hoop stress $\sigma_{\theta\theta}$ are normalized to the yield stress and are plotted as functions of the radial distance r divided by the outer radius R. These distributions are illustrated at four different time increments. The initial nucleus is shown by a white strip. The brown domain corresponds to the grown part of the α precipitate whereas the blue strip indicates the zone of plastic activity in the matrix phase. The domains are delimited by vertical dotted lines. The plastic zone size can be seen to increase as the precipitate grows. The hoop stress exhibits a steep increase at the $\alpha - \beta$ interface, $r = r_{int}$, which is the phase field counterpart of the discontinuity expected in the sharp interface model. The main feature of the stress distributions is that stresses as predicted by the interpolation and Voigt homogenisation almost coincide in the β matrix and strongly differ inside the precipitate. The homogenisation model predicts constant stress values inside the inclusion, in contrast to the strongly varying stress field provided by the interpolation model.

This can be understood by looking at the distribution of the plastic strain components $\varepsilon^p_{rr}, \varepsilon^p_{\theta\theta}$. According to the interpolation model, the plastic strain components are obtained by integrating the flow rule (16). In contrast, the plastic strain is defined by Eq. (31) in the homogenisation model. When the α phase starts growing, the stress level increases in the matrix due to the eigenstrain of the particle. The von Mises equivalent stress reaches the threshold value σ^0_β and plasticity starts flowing in the blue domain around the particle. As the particle continues growing, the interface propagates through the plastic zone of the matrix. As a result the α phase inherits (or not, depending on the model) some plastic deformation from the matrix phase. According to the interpolation scheme, a unique variable $\underset{\sim}{\boldsymbol{\varepsilon}}^p$ is defined and is therefore "transmitted" from one phase to the other. This explains why residual plastic deformation is observed within the α phase, even though it behaves purely elastically, as illustrated by the top part of Fig. 4. The amount of plastic strain inherited by the α phase from the matrix can be seen to increase when the particle size increases.

In contrast, according to the homogenisation model, the mixture rule (30) for the plastic strain in the precipitate implies that plastic strain inherited from the β matrix is progressively forgotten when ϕ asymptotically reaches the value 0. This explains why the plastic strain value inherited from the matrix is only visible in the diffuse interface region and in the β phase, and steeply decreases when leaving the interface in the α phase, as illustrated by the profiles in the bottom part of Fig. 4.

The radial strain profiles are shown in Fig. 5 according to the interpolation and homogenisation models. The latter predicts constant strain inside the precipitate. The solutions of the two models are found to be very close in the matrix. The difference in total strain on both sides of the interfaces is responsible for a difference in the so-called coherence energy $\mathcal{E}_{\text{coh}}$ defined as the elastic energy necessary to keep both lattices coherent across the interface [5, 23]. Its analytical expression and the evolution of the coherence energy with time during growth is shown in the upper right corner of Fig. 5.

The corresponding concentration profiles are given in Fig. 6. They show slight differences found in the precipitate according to the phase field model. They remain very close to each other in the matrix phase. The differences in elastic and coherence energies for both models illustrated in the upper right corner of Fig. 6 lead to different jumps of concentrations on each side of the interface in the form

$$c^{int}_{\alpha,\beta} = a_{\alpha,\beta} + (\mathcal{E} + \frac{\gamma}{R})/(k(a_\alpha - a_\beta)) \tag{46}$$

where

$$\mathcal{E} = f_{e,\alpha} - f_{e,\beta} - \mathcal{E}_{\text{coh}}, \quad \text{with}$$
$$\mathcal{E}_{\text{coh}} = \underset{\sim}{\boldsymbol{\sigma}}_\beta : (\underset{\sim}{\boldsymbol{\varepsilon}}^{\text{int}}_\alpha - \underset{\sim}{\boldsymbol{\varepsilon}}^{\text{int}}_\beta) \tag{47}$$

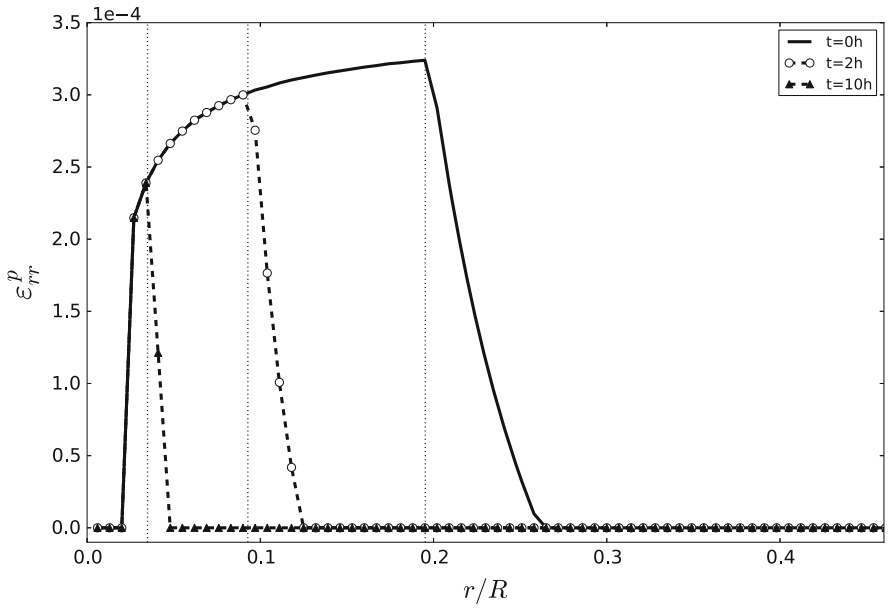

Interpolation model

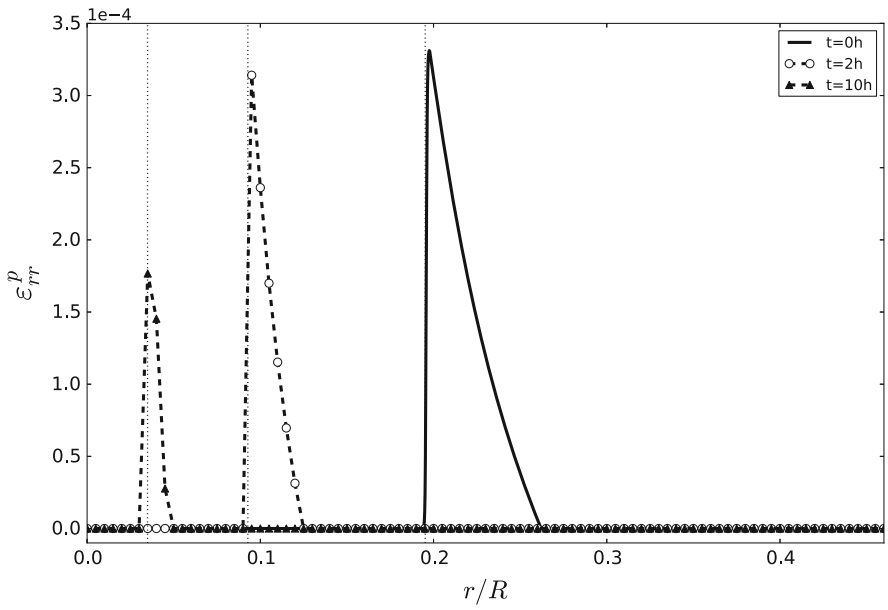

Voigt homogenisation model

Fig. 4 Plastic deformation distribution in a spherical precipitate embedded in a concentric spherical matrix as a function of the normalized radial distance r/R as computed at three different time steps for the interpolation model (top) and for the Voigt homogenisation model (bottom).

In particular, c_β^{int} is found to be slightly higher in the interpolation model than in the homogenisation model which induces a slightly less steep concentration gradient in the matrix, as shown in Fig. 6.

In order to examine the effect of stored elastic energy on the diffusional growth of a coherent spherical precipitate into a supersaturated matrix, the time evolution of the precipitate radius, normalized by the matrix radius r_{int}/R, is shown in Fig. 7 for the two models. A parabolic law describes the particle growth in both cases but with two different kinetic constants. The square of the precipitate radius increases linearly with time $\Delta e = K\sqrt{t}$. The found values for the coefficient K are: $K = 1.38 \times 10^{-9}$ ms^{-1} for the purely elastic model, $K = 1.12 \times 10^{-9}$ ms^{-1} for the elastoplastic homogenization model and $K = 10^{-9}$ ms^{-1} for the

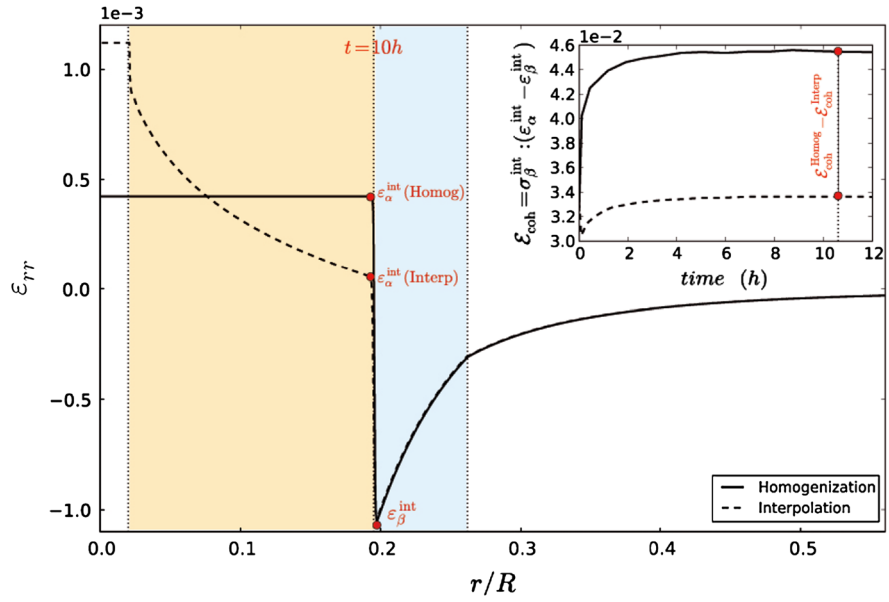

Fig. 5 Total strain distribution in a spherical precipitate embedded in a concentric spherical matrix as a function of the normalized radial distance r/R as computed at $t = 0$ hours for the interpolation model (dotted line) and for the Voigt homogenisation model (dark line).

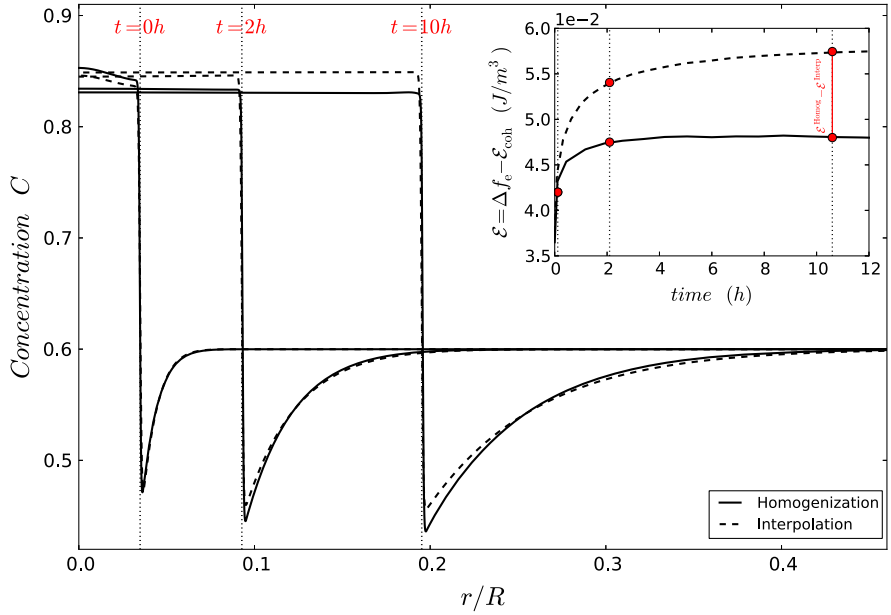

Fig. 6 Composition profile associated with the growth of an isolated coherent precipitate into a supersaturated matrix, according to the interpolation (dotted line) and homogenisation models (dark line) at three distinct time steps. The matrix/precipitate interface lies at $r/r_{\text{int}} = 1$ indicated by the vertical dotted line.

elastoplastic interpolation model. The reason for such different kinetics stems from the difference in stored elastic energy close to the interface induced by different plastic strain values. As shown in [5] for a dilatational misfit in the particle, plastic deformation leads to a slowdown of the growth kinetics compared to sole elasticity due to a flattening of the concentration profile in the matrix induced by relaxed stresses, as discussed before. The strain jump at the interface shown in Fig. 5 is higher according to the homogenisation model than in the interpolation model which explains the faster kinetics predicted by the former model. In other words, the higher stored elastic energy obtained with the homogenisation model leads to faster kinetics.

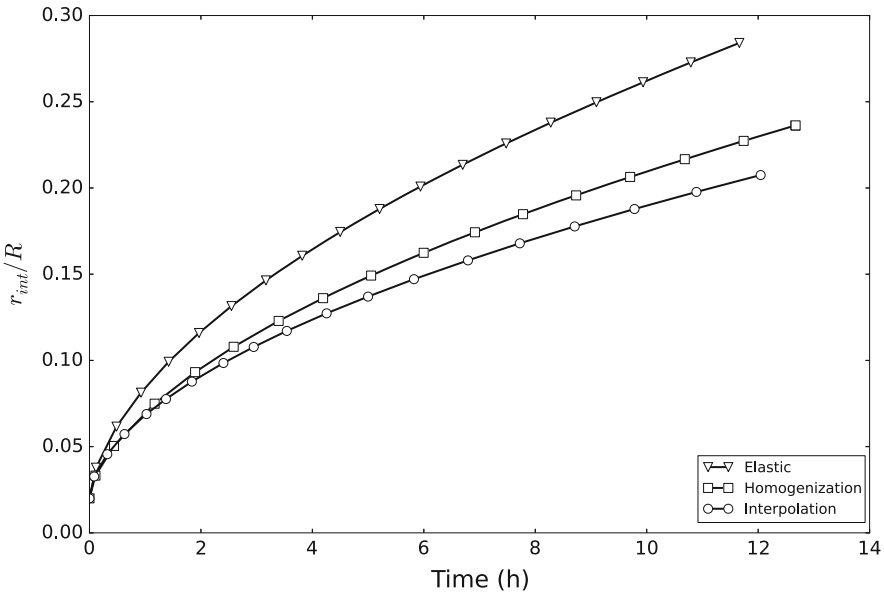

Fig. 7 Growth kinetics of a misfitting spherical precipitate in an isotropic infinite matrix. Two finite element calculations have been performed according to the interpolation and homogenisation models.

3.3 Microstructural evolution coupled to plastic activity

The phase field simulation of Ostwald ripening of a population of α precipitates embedded in a β-matrix is considered in this section, including the impact of elastoplastic deformation on the process. Ostwald ripening is a process related to the coarsening of one phase dispersed in a matrix phase. It is generally the last stage of a first-order phase transition in a two-phase region. The first stage is nucleation when a new phase forms from the mother phase, maintained in a supersaturated state. As the supersaturation decreases due to particle growth, the nucleation barrier and the stable cluster size increase. The system usually forms a microstructure with particles in a matrix. Even after full exhaustion of the driving force, the particles in the matrix are not in thermodynamic equilibrium. The system can further decrease its total free energy by decreasing the overall interface area between the particles and the matrix. The decrease of total interface area progresses by a process where the large particles grow at the expense of the smaller particles. The average size of the particles of the dispersed phase increases during coarsening due to diffusion through the matrix phase, and their total number decreases.

A square area has been meshed with 250×250 linear quadrangular elements. Several solid particles ($\phi = 1$) of different shapes and radii were randomly distributed in the matrix ($\phi = 0$). The initial solute compositions of both phases are homogeneous and set to be equal to $c_0 = 0.5$. The simulations are performed under plane strain conditions. Periodic boundary conditions are applied to the concentration and phase fields. Periodicity is also enforced to the mechanical variables ensuring here a vanishing mean stress, by means of a special finite element described in [8].

The simulated results for the Ostwald-ripening process are shown in Fig. 8 and 9, for the interpolation and homogenisation models respectively. In each case, the top figures illustrate the coarsening of the particles, i.e. the growth and coalescence of some particles and the disappearance of other ones. In both simulations, only two particles remain after 5 h. The kinetics is slightly faster for the homogenization than for the interpolation model.

The simulations also provide the field of cumulative plastic strain p defined as:

$$\dot{p} = \sqrt{\frac{2}{3}\underset{\approx}{\dot{\varepsilon}}^p : \underset{\approx}{\dot{\varepsilon}}^p} \tag{48}$$

at different time steps, see the bottom images of Figs. 8 and 9. At the final stage, the homogenisation model predicts very limited zones of residual plastic strain due to the sweeping of plastic strain by the interface. In contrast a complex field of plastic deformation is found to pertain according to the interpolation model.

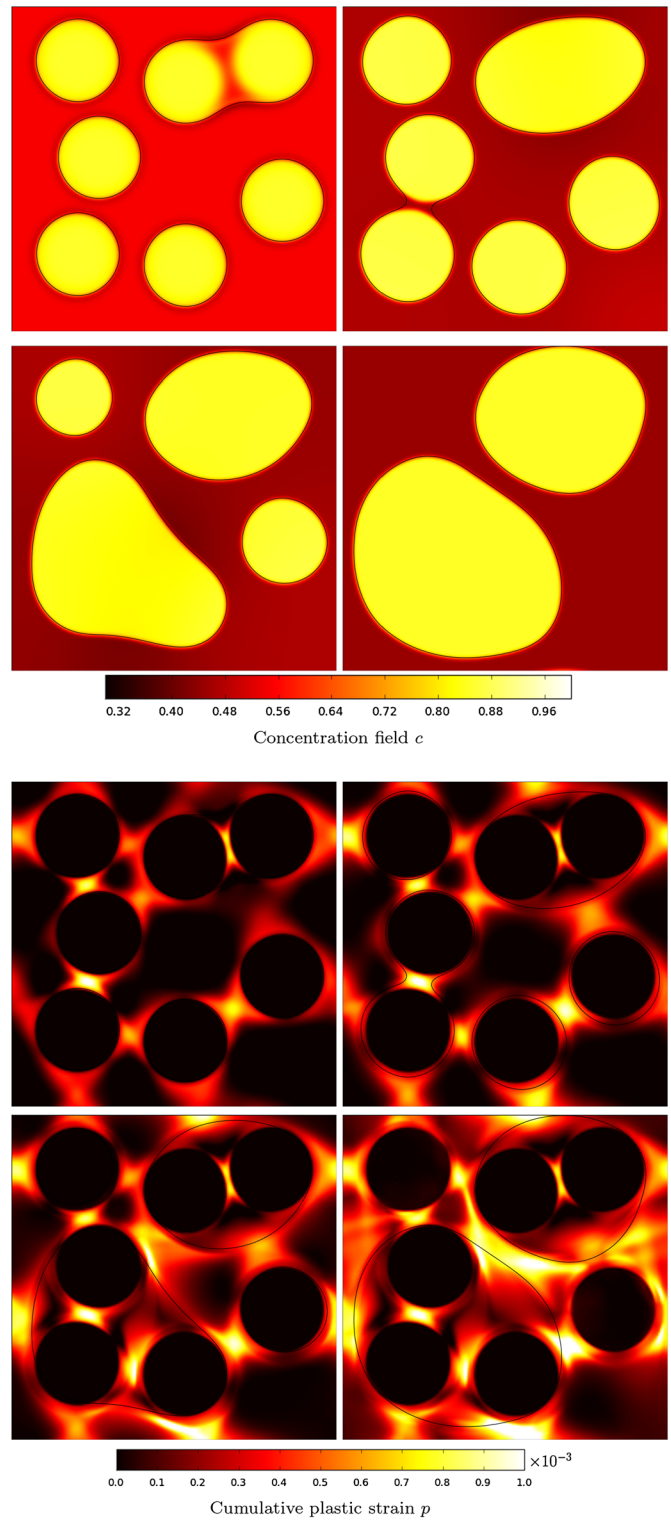

Fig. 8 Time history of Ostwald ripening process in the case of total inheritance between the new elastic formed phase and the parent plastic phase (interpolation model): phase field and field of cumulative plastic strain at the time steps $t = 0$, 1.7, 2.5, 5 h. The black lines in the bottom part denote the $\phi = 0.5$ iso-lines.

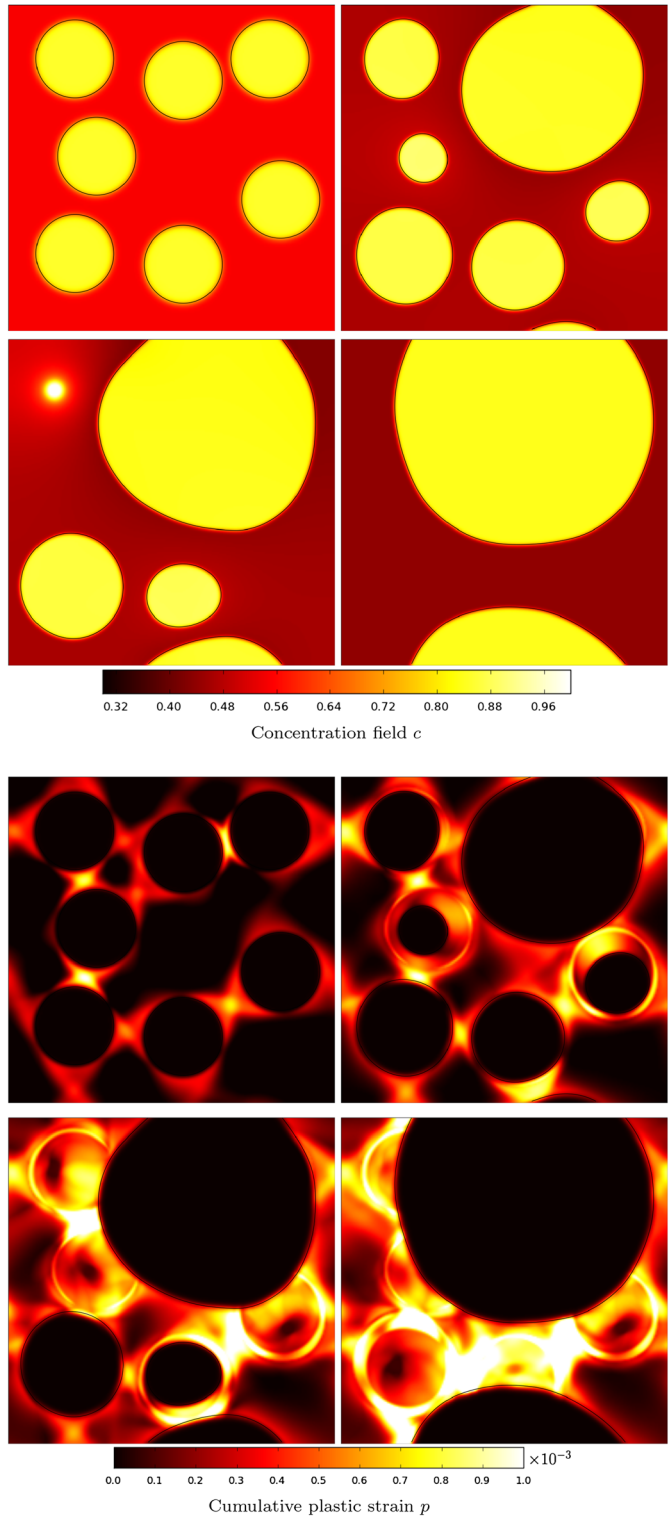

Fig. 9 Time history of Ostwald ripening process in the absence of inheritance between the new elastic formed phase and the parent plastic phase (homogenisation model): phase field and field of cumulative plastic strain at the time steps $t = 0, 0.25, 1, 5$ h.

As a result, the material swept by the phase transformation front is full of residual stresses. Residual stresses are much more limited for the homogenisation model. In particular, when the α phase will have spread over the whole domain, it is expected that the interpolation model will predict residual plastic strains and stresses inside the domain whereas the homogenisation will predict a new virgin state in the domain. This represents a major difference between both approaches. The relevance of both situations to the physical reality could be investigated by means of residual stress or strain field measurements with sufficient accuracy.

4 Conclusion

Recent advances in phase field modeling involve the nonlinear mechanical behaviour of materials during phase transformation. Two main classes of such models have been distinguished, namely the interpolation models relying on a single set of constitutive equations and interpolation of material parameters, and the homogenisation models that are based on the mixture of free energy and dissipation potentials associated with distinct behaviours of the phases. The two model classes have been shown to exhibit opposite behaviour regarding the question of inheritance of plastic deformation during phase transformation. As a rule, according to interpolation models, the plastic strain that occurred in the mother phase due to prior straining or induced by the local stresses arising at the vicinity of the interface, was shown to be inherited by the new phase after the passing of the interface. This means that the new reference state for computing elastic stresses is that of the parent phase. In contrast, according to homogenisation models, fading memory of plastic strain is observed due to the fact that the plastic strain tensor is expressed as an explicit weighted function of the plastic strain tensors attributed to each phase at each material point. This distinct behaviour of each model class has been shown to result in different residual plastic strain and stress fields after transformation. Residual stresses are minimized when using homogenisation models. Interpolation models lead to a non-vanishing residual plastic strain field, even after complete phase transformation. This residual plastic strain field reflects the history of growth and coalescence of precipitates embedded in an elastoplastic matrix.

Finite element simulation results were given in the case of a misfitting elastic precipitate phase growing within an elastoplastic von Mises matrix. A slowdown of transformation kinetics due to plasticity compared to purely elastic behaviour was observed and related to the strain relaxation induced by plasticity close to the interface [5]. The homogenisation was shown to lead to a slightly faster kinetics than the interpolation models due to the fact that the inheritance of plastic deformation in the latter model allows for higher strain relaxation. This slowdown in the growth kinetics does not reflect the pipe diffusion effects induced by dislocations which would rather lead to significant acceleration of the kinetics in alloys. Pipe diffusion effects could be introduced in the modelling by means of a dependence of diffusion coefficients on dislocation density. Although only two-dimensional axisymmetric or plane strain simulations were provided in this work, the fundamental difference in the resulting inheritance behaviour of the two classes of models remains in the 3D case, because it lies in the mathematical formulation of the models. The axisymmetric example already addresses spherical precipitate shape but random distributions of growing second phase in an elastoplastic matrix must be considered in the future.

It is anticipated that the actual behaviour of engineering materials lies between that of total inheritance of plastic deformation and no inheritance at all. It will therefore be necessary to develop phase field models combining features of both model classes investigated in this work and leading to the possibility of partial inheritance.

Hardening laws were formulated in the constitutive models but not used in the simulation because the existence of hardening raises the question of inheritance of dislocation microstructures after the passing of an interface, which is a different question from that of the inheritance of plastic deformation. The latter solely represents a change in the reference local configuration for the computation of elastic stresses. The question of inheritance of hardening microstructures will be the subject of future work both in the case of the phenomenological constitutive equations presented in the present work and for phase field dislocation models proposed in [19]. Also, rate-independent plasticity only was considered in the

present work to avoid mixing too many phenomena in the discussion. The presented model formulations are general and include viscoplastic behaviour that is more realistic for diffusional phase tranformation and will be used in the future.

The question of inheritance of plastic strain gradients, i.e. accumulation of geometrically necessary dislocations close to boundaries could also be modelled within a coupled phase field/strain gradient plasticity approach as proposed in [11].

Acknowledgments The authors acknowledge the financial support of the French Agence Nationale de la Recherche (ANR) under reference ANR-BLAN08-1-321567 (project Couphin).

References

1. Abrivard G, Busso E, Forest S, Appolaire B (2012) Phase field modelling of grain boundary motion driven by curvature and stored energy gradients. Part I: theory and numerical implementation. Philos Mag 92:3618–3642
2. Abrivard G, Busso E, Forest S, Appolaire B (2012) Phase field modelling of grain boundary motion driven by curvature and stored energy gradients. Part II: application to recrystallisation. Philos Mag 92:3643–3664
3. Ammar K, Appolaire B, Cailletaud G, Feyel F, Forest S (2009) Finite element formulation of a phase field model based on the concept of generalized stresses. Comput Mater Sci 45:800–805
4. Ammar K, Appolaire B, Cailletaud G, Forest S (2009) Combining phase field approach and homogenization methods for modelling phase transformation in elastoplastic media. Eur J Comput Mech 18:485–523
5. Ammar K, Appolaire B, Cailletaud G, Forest S (2011) Phase field modeling of elasto-plastic deformation induced by diffusion controlled growth of a misfitting spherical precipitate. Philos Mag Lett 91:164–172
6. Anders D, Weinberg K (2011) Numerical simulation of diffusion induced phase separation and coarsening in binary alloys. Comput Mater Sci 50:1359–1364
7. Barbe F, Quey R, Taleb L, Souza de Cursi E (2008) Numerical modelling of the plasticity induced during diffusive transformation. An ensemble averaging approach for the case of random arrays of nuclei. Eur J Mech A/Solids 27:1121–1139
8. Besson J, Cailletaud G, Chaboche JL, Forest S, Blétry M (2009) Non-linear mechanics of materials. Series: solid mechanics and its applications, vol 167. Springer, New York. ISBN: 978-90-481-3355-0
9. Bourne J, Atkinson C, Reed R (1994) Diffusion controlled growth in ternary systems. Metall Mater Trans A 25:2683–2694
10. Cha PR, Kim J, Kim WT, Kim S (2009) Effect of transformation induced stress and plastic deformation on austenite/ferrite transition in low carbon steel. Plasticity 2009:376–378
11. Cottura M, Le Bouar Y, Finel A, Appolaire B, Ammar K, Forest S (2012) A phase field model incorporating strain gradient viscoplasticity: application to rafting in Ni-base superalloys. J Mech Phys Solids 60:1243–1256
12. Durga A, Wollants P, Moelans N (2013) Evaluation of interfacial excess contributions in different phase-field models for elastically inhomogeneous systems. Model Simul Mater Sci Eng 21:055018
13. Eiken J, Böttger B, Steinbach I (2006) Multiphase-field approach for multicomponent alloys with extrapolation scheme for numerical application. Phys Rev E 73:066122
14. Forest S (2008) The micromorphic approach to plasticity and diffusion. In: Jeulin D, Forest S (eds) Continuum models and discrete systems 11. Proceedings of the international conference CMDS11, Les Presses de l'Ecole des Mines de Paris, Paris, pp 105–112
15. Forest S (2009) The micromorphic approach for gradient elasticity, viscoplasticity and damage. ASCE J Eng Mech 135:117–131
16. Ganghoffer J, Denis S, Gautier E, Simon A, Simonsson K, Sjöström S (1991) Micromechanical simulation of a martensitic transformation by finite elements. J Phys IV (France) 1:C4-77-82
17. Gaubert A, Finel A, Le Bouar Y, Boussinot G (2008) Viscoplastic phase field modellling of rafting in Ni base superalloys. In: Continuum models and discrete systems CMDS11. Mines Paris Les Presses, Paris, pp 161–166.
18. Gaubert A, Le Bouar Y, Finel A (2010) Coupling phase field and viscoplasticity to study rafting in Ni-based superalloys. Philosophical Magazine 90:375–404
19. Geslin P, Appolaire B, Finel A (2014) Investigation of coherency loss by prismatic punching with a nonlinear elastic model. Acta Mater 71:80–88
20. Greenberg B, Volkov A, Kruglikov N (2001) Composite-like behavior of alloys ordered after severe cold deformation. Phys Metals Metallogr 92:167–178
21. Guo X, Shi S, Ma X (2005) Elastoplastic phase field model for microstructure evolution. Appl Phys Lett 87:221910-1-3
22. Gurtin M (1996) Generalized Ginzburg−Landau and Cahn−Hilliard equations based on a microforce balance. Phys D 92:178–192
23. Johnson WC, Alexander JID (1986) Interfacial conditions for thermomechanical equilibrium in two-phase crystals. J Appl Phys 9:2735–2746
24. Khachaturyan A (1983) Theory of structural transformations in solids. Wiley, New York
25. Kim S, Kim W, Suzuki T (1998) Interfacial compositions of solid and liquid in a phase-field model with finite interface thickness for isothermal solidification in binary alloys. Phys Rev E 58(3):3316–3323
26. Kim S, Kim W, Suzuki T (1999) Phase-field model for binary alloys. Phys Rev E 60(6):7186–7197
27. Kouznetsova V, Geers M (2007) Modeling the interaction between plasticity and the austenite-martensite transformation. Int J Multiscale Comput Eng 5:129–140
28. Kundin J, Raabe D, Emmerich H (2011) A phase-field model for incoherent martensitic transformations including plastic accommodation processes in the austenite. J Mech Phys Solids 59:2082–2102
29. Lemaitre J, Chaboche JL (1994) Mechanics of solid materials. University Press, Cambridge, UK

30. Louchet F, Hazotte A (1997) A model for low stress cross-diffusional creep and directional coarsening of superalloys. Scr Mater 37:589–597
31. Nemat-Nasser S, Hori M (1999) Micromechanics: Overall properties of heterogeneous solids, 2nd edn. Elsevier Science Publishers, Amsterdam
32. Qu J, Cherkaoui M (2006) Fundamentals of micromechanics of solids. Wiley, Hoboken
33. Sanchez-Palencia E, Zaoui A (1987) Homogenization techniques for composite media. Lecture notes in physics vol, 272, Springer, Berlin
34. Spatschek R, Eidel B (2013) Driving forces for interface kinetics and phase field models. Int J Solids Struct 50:2424–2436
35. Steinbach I (2009) Phase field models in materials science. Model Simul Mater Sci Eng 17:1–31
36. Steinbach I, Apel M (2006) Multi phase field model for solid state transformation with elastic strain. Phys D 217:153–160
37. Steinbach I, Apel M (2007) The influence of lattice strain on pearlite formation in Fe-C. Acta Mater 55:4817–4822
38. Steinbach I, Shchyglo O (2011) Phase-field modelling of microstructure evolution in solids: perspectives and challenges. Curr Opin Solid State Mater Sci 15:87–92
39. Ubachs R, Schreurs P, Geers M (2004) A nonlocal diffuse interface model for microstructure evolution of tin-lead solder. J Mech Phys Solids 52:1763–1792
40. Ubachs R, Schreurs P, Geers M (2005) Phase field dependent viscoplastic behaviour of solder alloys. Int J Solids Struct 42:2533–2558
41. Wang Y, Chen LQ, Khachaturyan A (1993) Kinetics of strain-induced morphological transformation in cubic alloys with a miscibility gap. Acta Metallurgica et Materialia 41:279–296
42. Wang Y, Khachaturyan A (1995) Shape instability during precipitate growth in coherent solids. Acta Metall Mater 43(5):1837–1857
43. Weinberg K, Böhme T, Müller W (2009) Kirkendall voids in the intermetallic layers of solder joints in MEMS. Comput Mater Sci 45:827–831
44. Z-set package: Non-linear material & structure analysis suite. www.zset-software.com. (2013)
45. Zaoui A (2002) Continuum micromechanics: survey. ASCE J Eng Mech 128:808–816
46. Zhou N, Shen C, Mills M, Wang Y (2008) Contributions from elastic inhomogeneity and from plasticity to γ' rafting in single-crystal Ni-Al. Acta Mater 56:6156–6173